TITLE PAGE (Original Research)

Title

Improved Durability of a Modular Axial Fixator for Stable and Unstable Proximal Femoral Fractures: A Patient-Specific Finite Element Analysis

Running Head (abbreviated title)

FEA of a modular axial fixator employed in cases of proximal femoral fracture

Author(s)

[1,*] H. Kursat CELIK, PhD, Assoc. Prof.	hkcelik@akdeniz.edu.tr	ORCID: 0000-0001-8154-6993
[2] Mustafa IÇEN, MD.	micen@akdeniz.edu.tr	ORCID: 0000-0001-6338-146X
[2] Hakan OZDEMIR, MD, Prof.	hakanozdemir@akdeniz.edu.tr	ORCID: 0000-0003-3723-1606
[3] Allan E.W. RENNIE, PhD, Prof.	a.rennie@lancaster.ac.uk	ORCID: 0000-0003-4568-316X

[1,] Dept. of Agr. Machinery and Technology Engineering, Akdeniz University, Antalya, Turkey*
[2] Dept. of Orthopaedics and Traumatology, Fac. of Medicine, Akdeniz University, Antalya, Turkey
[3] School of Engineering, Lancaster University, Lancaster, United Kingdom

Corresponding Author(s)

[1,*] H. Kursat CELIK, PhD, Assoc. Prof. hkcelik@akdeniz.edu.tr ORCID: 0000-0001-8154-6993
[1,] Dept. of Agr. Machinery and Technology Engineering, Akdeniz University, Antalya, Turkey*

Conflict of Interest Statement

The authors declare that they have no known competing financial interests or personal relationships that could have appeared to influence the work reported in this paper.

Keywords: Modular Axial Fixator, Proximal Femoral Fracture, Implant Design, Durability, Finite Element Analysis

Improved Durability of a Modular Axial Fixator for Stable and Unstable Proximal Femoral Fractures: A Patient-Specific Finite Element Analysis

ABSTRACT

Femoral neck fractures, comprising 8-10% of all bodily fractures in the elderly, often necessitate alternatives to extensive surgical interventions. Despite limited research, external fixators are considered promising. This study evaluates the design and durability of a novel Modular Axial Fixator (MAF) for stable and unstable proximal femoral fractures, using numerical method-based engineering analysis. Employing patient-specific CT scan data, 3D solid modelling, and finite element analysis (FEA), the MAF-bone fixation is examined in eight simulation scenarios under static loading conditions. FEA results show a peak femur head displacement of 7.429 mm in FEA 001, with Schanz screw no. 2 reaching the maximum equivalent stress at 431.060 MPa in FEA-006. Notably, the 7.429 mm displacement improves stability compared to previous studies, yet interfragmentary movement surpasses the 100-200 μm reference range for primary fracture healing, posing challenges to direct healing despite enhanced stability. This study validates the durability of the innovative MAF for femoral neck fractures through engineering simulations. It contributes to understanding MAF durability issues, with implications for improving medical implant design in the industry. Simulation results offer opportunities for optimising structure and production, enhancing the MAF's design, and ultimately benefiting medical implant manufacturing.

Keywords: Modular Axial Fixator, Proximal Femoral Fracture, Implant Design, Durability, Finite Element Analysis

1. INTRODUCTION

Proximal femoral fractures constitute a significant proportion of hospitalisations in trauma cases, with an overwhelming majority of patients (more than 90%) aged 50 years and above. This also represents approximately 8-10% of all bodily fractures. The incidence of these fractures is two to three times higher in females compared to the male population. They are categorised based on the anatomical location into femoral neck fractures, intertrochanteric fractures, and subtrochanteric fractures. Each type of fracture necessitates specialised treatment methods and presents its own set of complications and intricacies regarding the optimal management approach [1].

Femoral neck fractures include injuries that involve the area between the head of the femur and the intertrochanteric line [2]. Pauwels categorised femoral neck fractures based on the angle of inclination of the fracture line as measured from the horizontal on an anteroposterior radiograph, which was introduced in 1935, and to clarify, this classification system divides fractures into three distinct types: Pauwels Type I (<30°), Type II (30° ~ 50°), and Type III (>50°) [3–5].

The primary objective of fracture treatment is to achieve a prompt and enduring union of the fracture, ensuring full function of the injured limb, and facilitating the rapid rehabilitation of the patient. However, attaining and sustaining stable fixation in geriatric patients can pose significant challenges due to osteoporotic bone. Common surgical approaches employed in the treatment of intertrochanteric fractures of the femur (ITFF) include the dynamic hip screw (DHS), Proximal Femoral Nail (PFN), bipolar hemiarthroplasty (BPH), and External Fixation (EF). Among these techniques, EF has been identified as having substantial advantages, including significantly reduced operating times, decreased intraoperative blood loss, and the need for sedation only in high-risk patients [6]. On the contrary, although external fixation was first utilised in the 1950s for treating related fractures, a high incidence of postoperative complications, such as pin loosening, infection, and mechanical failure of the fixator, led surgeons to reconsider its use. However, the development of newly designed external fixators has revived interest in external fixation as a viable treatment option for proximal femoral fractures. Recent studies on these modern fixators have demonstrated that external fixation can yield results similar to, or even better than, those achieved with traditional internal fixation techniques [7]. Existing literature on the use of external fixators for femoral neck fracture management reveals a consensus regarding their potential applicability in situations where the patient's overall condition precludes extensive surgical intervention [8–13]. It is worth noting that these fractures often exhibit a severe and potentially fatal progression. Despite the scarcity of published research, the prevailing opinion suggests that external fixators may serve as a viable alternative when the patient's health status does not permit major surgical procedures. In their studies conducted in 2002 and 2003, Özdemir et al. employed the Modular Axial Fixator (MAF) to manage proximal femur fractures in patients with an unfavourable overall health condition and a high surgical risk (American Society of Anaesthesiologists (ASA) Grade III-IV) [14,15]. Furthermore, the researchers introduced a pilot study on the design and performance evaluation of a MAF tool in 2016 [16]. Based on the evaluation of the data collected in their study, they reported that the utilisation of external fixation for fractures occurring in the proximal region of the femur can be considered a conventional treatment approach rather than an alternative option when viewed through a biomechanical lens. Additionally, the findings suggest that by implementing certain modifications to the existing systems, this method can also prove to be a dependable solution for managing unstable fractures. It should be emphasised here that the primary distinction of this study from the previous one cited in reference 16 lies in the alteration of the geometric shapes, dimensions, and an additional component. By incorporating the insights and feedback provided in this reference, it was prompted to make updates and modifications to attain innovative design specifications for testing and developing the durability of the newer design through a more realistic Finite Element Analysis (FEA) approach, incorporating complete components, including screws, screw treats etc. rather than relying solely on oversimplified component geometries.

In light of the aforementioned context, indicating a gap in addressing the development of new external fixator designs suitable for secure utilisation in surgeries pertaining to proximal femur fractures, it is imperative to consider the iterative nature of the product design process. This process commences with a decision or set of requirements and culminates in the creation of a tangible product or process. Within these iterative phases, the structural analysis of the conceptualised product plays a crucial role, providing essential data regarding the product's durability to determine optimal design parameters. However, the experimental analysis of multi-part complex structures is often impractical within the design sequence. In such instances, Computer-Aided Design and Engineering (CAD/CAE) analysis offer valuable advantages to designers. CAE analysis, based on numerical methods such as the finite element method (FEM), can be employed for evaluating the mechanical performance of fracture fixation. By opting for FEM-based analysis (FEA) rather than conducting experiments, there is the advantage of time, assessing new implants and fixation approaches before implementation. Moreover, it facilitates the evaluation of stresses and deformations occurring within the bone or at the interfaces of bone, implant, or fixator components. These aspects are often challenging, if not impossible, to measure experimentally. Consequently, employing FEA may offer predictions regarding the clinical performance of implants and fixators. The confidence level in simulation predictions, therefore, relies on a valid computerised fracture model using FEA, enabling the investigation of the influence of critical mechanical factors on the stability of femoral neck fracture fixations [17–23].

The aim of this study is to provide an examination of the design and durability of a recently introduced modular axial fixator intended for addressing both stable and unstable proximal femoral fractures, employing advanced CAE applications. In order to achieve this aim, engineering simulations based on the FEM were employed to assess the durability of the recently designed MAF. More precisely, the emphasis was placed on evaluating deformation and stress

distribution within the fixator to ascertain its robustness and reliability in meeting the fixation requirements essential for fracture healing.

2. MATERIALS AND METHODS

2.1. Solid Model of the MAF and Bone Fixation

In this section, the solid model of the MAF and bone fixation is presented. The purpose of this model is to provide a detailed representation of the MAF and its interaction with the bone fixation system. To create an accurate digital model, the femur bone was reconstructed using computerised tomography (CT) data from a patient. The CT scan procedure was conducted at Akdeniz University using a Siemens go.Up CT device (Siemens, Munich, Germany). The scan parameters were set as follows: 100 KV, 36 mA, a slicing distance of 0.6 mm, resulting in a total of 812 axial slices. The patient, a female, of height of 158 cm and weight of 70 kg. A thorough evaluation of the CT scan was performed by an experienced radiologist and an orthopaedic surgeon, who confirmed the absence of any bone lesions. The patient provided written consent for the anonymous use of her imaging data. The femur solid model was created by segmenting the soft tissues from the bony structures using Mimics Medical software (Materialise, Leuven, Belgium). To refine and further modify the model, SolidWorks (Dassault Systèmes, Paris, France), a 3D parametric solid modelling software, was employed. Subsequently, stable and unstable fracture models were developed and attached a parametrically designed MAF to the femur models. In total, eight different MAF configurations were prepared for analysis in both stable and unstable femoral neck fracture scenarios (Pauwels Type II and III). Figure 1 presents a visual representation of the model details utilised in the FEA scenarios.

(**Figure 1.** Visual representation of the model details utilised in the FEA)

2.2. Material Properties

A comprehensive review of the literature on FEA of femur bone structures was conducted, with a careful evaluation of the deformation behaviour of these structures using the assigned material properties discussed in previous research. While a consensus on specific material properties for bone structures could not be reached due to limitations in material modelling, certain experimental studies offered valuable insights into the material properties of the femur bone for numerical analysis. This study specifically focused on analysing the material properties of cortical and trabecular bones separately, as the cortical bone exhibits greater density and strength compared to the porous trabecular structure. To fulfil the primary objective of this study, a homogeneous isotropic linear elastic material model was adopted for the materials used in the FEA scenarios, which adequately served the purpose. Following the literature references, the elastic modulus calculations for cortical and trabecular bone were performed based on Hounsfield units (HU). The Poisson's ratio was assumed to remain constant throughout the calculations. Equation 1 was employed to determine the real density, taking into account the linear correlation between bone apparent density and HU. The elastic modulus of the femur bone structure was then calculated using Equation 2 [24–26].

In terms of the FEA setup, the bar modules and leg support were assigned as the material Aluminium 7075-T6, while the Schanz screws were made of Medical Grade Stainless Steel 316 LVM [27]. Table 1 provides an overview of the material properties utilised in the FEA.

$$\rho = HU\ 750^{-1} \tag{1}$$

$$E = \begin{cases} 1904\ \rho^{1.64}, & \rho < 0.946\ (Trabecular) \\ 2065\ \rho^{3.09}, & \rho \geq 0.946\ (Cortical) \end{cases} \tag{2}$$

Where; HU: Hounsfield units (HU) measured from patient's CT data, E: Elastic Modulus (MPa); ρ: Real density (g cm^{-3})

Table 1. The material properties utilised in the FEA

Parameters	Unit	Model Components			
		Cortical Bone	Trabecular Bone	Schanz Screws (S.S. 316 LVM)	Bar Modules and Leg Support (Al 7075-T6)
Modulus of Elasticity	(MPa)	21464	1320	200000	72000
Poisson's Ratio	(-)	0.3	0.3	0.33	0.33
Density	(kg m^{-3})	2130	800	8000	2800

2.3. Boundary Conditions, Mesh Structure and Internal Verification

The loading magnitude was calculated by taking into account the subject's body weight (BW: 70 kg). The loading scenarios assumed that the patient was standing on their injured leg immediately after the fracture fixation surgery, and the femur was subjected to axial (vertical) loading during this static stance on a single leg. While it is acknowledged that muscles and other soft tissues also provide support to the femur, the main source of loading is body weight, and the hip joint serves as the primary weight-bearing structure in the human body. In this research, the authors compared various approaches to modelling and analysing the resultant force using biomechanical models described in existing literature. A comprehensive study conducted by Eschweiler et al. (2012) investigated the resultant force on the hip joint [28]. The biomechanical model employed for loading the femur in our study was adapted from their research. Consequently, for the FEA setup, the loading magnitude on the femur head structure was assigned as 1847 N (representing a magnitude of 2.69 of BW) with an associated angle of 18.47° (1752 N in vertical and 585 N in horizontal directions), which corresponds to the patient's weight of 70 kg. The femur bone was fixed at the knee joint, and the effect of Earth's gravity was taken into consideration. Another crucial parameter that affects the simulation results is the definition of contact between the components employed in the FEA. For this simulation study, sliding contact definitions (no-separation) were defined for the fracture fragments, screws, and bar module components. Bonded contact definitions were employed to represent the anatomical reality of the cortical and trabecular structures of the femur. In the study, a total of eight loading scenarios were established, taking into account stable and unstable proximal femur fracture fixation, with different leg support locations.

The mesh structure (Finite Element Model) was constructed using the meshing functions of the FEA code. Identical meshing parameters were assigned for each of the scenarios. To ensure accurate results, meshing approaches based on individual parts were utilised, with smaller element sizes specifically assigned to certain areas in the model, such as the screw thread zones in order to ensure precise results. The appropriate element size for the FE model was determined through preliminary trials. In order to assess the accuracy of the FE model and internally verify it, a skewness metric was employed. Figure 2 provides a comprehensive depiction of the boundary conditions, encompassing the forces exerted on the bone, loading scenarios, along with both visual and numerical intricacies of the FE model. After the pre-processing steps were completed, the solution processes were executed and documented on a Dell Precision M4800 series mobile workstation. The workstation incorporates an Intel Core i7-4910Q-2.9 GHz processor, 32 GB RAM, and an NVIDIA Quadro K2100M-2 GB DDR5 graphics card to ensure reliable and efficient analysis solving.

(Figure 2. Depiction of the boundary conditions, details of the FE model (mesh Structure) and loading scenarios)

3. RESULTS AND DISCUSSION

3.1. Equivalent stress and deformation outputs

A realistic, full-scale 3D model configuration of the MAF-femur fixation was successfully created in this study. These models were used for analysing the durability of the MAF-bone fixation. After the simulation process, numerical and visual outputs were obtained and recorded. The simulations visually demonstrated the deformation behaviour of the MAF-bone fixation under predefined loading conditions, while numerical results showed the stress and deformation magnitudes for the bone structure and fixator components. The simulation results exhibited logical deformation behaviour for all models, with the displacement (deformation) results being relatively similar to each other in corresponding stable and unstable fracture models. Regarding the loading direction, the femur head, which is the force application location and the furthest distance from the fixation point of the model, exhibited the highest global maximum displacement results. The maximum and minimum displacements were 7.429 mm for analysis FEA 001 and 7.362 mm for analysis FEA 006, respectively. The deformation values for the other components also indicated that there were no issues with the design of the MAF structure and bone fixation components under the predefined boundary conditions. For all eight analyses, the maximum stress results were observed in the Schanz screws. The maximum equivalent stress value among the eight analyses was 431.06 MPa for Schanz screw no: 2 in the FEA-006 scenario. The stress results also revealed that, although there was not much difference in the displacement results, the stress results were approximately twice as high for unstable fracture models compared to stable fracture models. This could be attributed to the fracture angle, as the screw-bone zone experienced a higher shear force effect in unstable fracture contact areas, even with the same force magnitude as stable fracture models. Table 2 and Figure 3 present the associated numerical outputs, along with plots illustrating the distribution of global (for entire model) maximum deformation and maximum equivalent stress.

Table 2. FEA numerical outputs: Maximum equivalent stress and maximum resultant deformation magnitudes

FEA Numerical Outputs	Stable Fracture								Unstable Fracture							
Components	**FEA - 001**		**FEA - 001b**		**FEA - 002**		**FEA - 003**		**FEA - 004**		**FEA - 004b**		**FEA - 005**		**FEA - 006**	
	MES* (MPa)	**MRD** (mm)**	**MES* (MPa)**	**MRD** (mm)**	**MES* (MPa)**	**MRD** (mm)**	**MES* (MPa)**	**MRD** (mm)**	**MES* (MPa)**	**MRD** (mm)**	**MES* (MPa)**	**MRD** (mm)**	**MES* (MPa)**	**MRD** (mm)**	**MES* (MPa)**	**MRD** (mm)**
Entire Model (Full Components Assembly)	238.29	7.429	238.620	7.427	239.360	7.423	240.710	7.424	413.530	7.366	414.740	7.365	424.180	7.364	431.060	7.362
Femur - Cortical Bone	150.49	7.125	154.570	7.118	150.610	7.120	159.630	7.122	306.880	7.110	307.530	7.107	306.400	7.110	308.200	7.106
Femur - Cortical Bone -Fracture Segment	122.35	7.460	123.420	7.427	122.610	7.403	123.590	7.433	247.400	7.366	247.760	7.363	242.960	7.366	248.910	7.362
Femur - Trabecular Bone	74.454	7.085	74.500	7.072	81.066	7.075	79.424	7.079	172.860	7.054	172.700	7.051	167.310	7.055	177.850	7.050
Femur - Trabecular Bone - Fracture Segment	65.162	7.379	65.171	7.376	65.480	7.350	66.732	7.362	95.950	7.314	96.789	7.311	114.310	7.315	115.830	7.311
Modular Bar (Al 7075-T6)	15.053	7.087	18.413	6.989	18.278	7.016	15.232	7.010	30.997	7.071	31.959	7.044	29.214	6.983	32.800	6.899
Leg Support (Al 7075-T6)	13.283	6.731	-	-	16.826	6.581	15.784	6.723	15.589	6.696	-	-	21.663	6.602	25.448	6.530
Schanz Screw No: 1 (S.S. 316 LVM)	119.28	7.110	119.970	7.103	124.230	7.080	126.080	7.109	221.060	7.042	219.410	7.041	214.790	7.043	226.990	7.040
Schanz Screw No: 2 (S.S. 316 LVM)	187.5	7.118	187.590	7.096	188.320	7.061	188.470	7.101	413.530	7.034	414.740	7.035	424.180	7.037	431.060	7.033
Schanz Screw No: 3 (S.S. 316 LVM)	238.86	7.019	239.620	7.016	244.360	6.984	240.710	7.011	381.000	6.952	389.720	6.969	386.420	6.954	390.220	6.950
Schanz Screw No: 4 (S.S. 316 LVM)	150.11	4.668	150.150	4.625	160.440	4.655	194.560	4.661	205.590	4.558	205.350	4.572	199.410	4.570	215.610	4.514
Schanz Screw No: 5 (S.S. 316 LVM)	110.39	4.628	110.770	4.416	122.600	4.443	124.800	4.623	123.320	4.456	121.060	4.470	126.780	4.468	127.270	4.409

**Max. Equivalent Stress (MES)*
***Max. Resultant Deformation (Displacement) (MRD)*

(**Figure 3.** Double axis chart representation and FEA visual outputs for global equivalent stress and displacement for stable and unstable fracture fixations)

Figure 3 illustrates the variation in numerical and visual results for maximum stress and deformation, which are separately presented in Table 2, consolidated within a single chart. In the figure, the analysis results from FEA-001 to FEA-003 indicate stable fracture fixations, whereas those from FEA-004 to FEA-006 represent unstable fracture fixations. The graph aims to demonstrate that stress concentrations decrease in unstable fracture fixation, while deformations (displacements) increase compared to stable fracture fixation. One possible reason for this phenomenon is the higher fracture angle, which allows for easier displacement under defined loading conditions in unstable fracture fixation, thereby exerting relatively less stress on the related component.

In the fixation procedure, while the Schanz screws assume the primary role in distributing maximum stress, it may be said that the modular bar serves as the principal element for load absorption and support, with the load being transferred through the Schanz screws to the modular bar. The eight simulation results confirmed that the modular bar worked according to its design specifications, demonstrating durability and stability under the predefined loading conditions. Furthermore, the Schanz screws exhibited stability and durability in withstanding the applied load. The stability of the results can be compared with a previous study conducted by Özdemir et al. (2016), where the analysed scenarios involving modular bar fixation showed total displacement values ranging approximately between 10 and 15 mm [16]. In contrast, this study recorded a displacement value of approximately 7.4 mm, which may indicate improved stability. Additionally, it can be stated that the observable impact of the leg support on the deformation behaviour of the MAF was not significant. It should be emphasised that, in this specific study, the leg support does not function as a load-bearing component. There were no specific boundary conditions defined for the bar. However, if a new simulation scenario is introduced that incorporates loading on the leg support, it may yield different outcomes.

3.2. Material Failure Evaluation

When evaluating damage (material failure) conditions, one can assess signs of damage by analysing the distribution of stress magnitudes on the components and comparing them to the material's damage threshold, which may be represented by the ultimate or yield stress point, depending on the material. For the purpose of this study, the damage threshold is defined as the material's yield stress point, which signifies the point at which permanent deformation (plastic deformation) takes place. In a stress analysis, it is crucial to calculate the factor of safety (FoS) in order to ensure the structural integrity and safety of a component or structure when subjected to expected loading conditions. In this study, the FoS for the MAF-bone fixation components was determined by dividing the material's yield stress value by the

calculated stress results obtained from the simulations. A FoS value below 1 indicates damage or material failure. The results of FoS calculations for individual components and FEA scenarios are presented in Figure 4. The calculation results revealed no evidence of failure in the MAF components, considering the failure threshold of the relevant materials. The minimum FoS calculated for the modular bar was 17.073 (FEA-006), indicating a high level of safety. Similarly, the minimum FoS value for the Schanz screws was 1.624 for Screw no: 2 in Scenario FEA 006. These results demonstrate that the MAF elements can withstand stress effectively under the specified loading conditions.

(Figure 4. Calculation of the factor of safety (FoS) by components)

In this FoS evaluation, it is important to emphasise a specific situation. While no signs of failure were observed for the modular bar and the Schanz screws, it was noted that there were excessive stress levels on the trabecular and cortical bone contacts at the regions where the screws hold the bone structures, namely the screw threads and fracture line zones. These elevated stress magnitudes suggest the presence of material damage. This observation is also reflected numerically in the FoS calculation results presented in Figure 4, where values below 1 indicate potential issues with the bone structures. The visual representation of the aforementioned situation is depicted in Figure 5. Upon closer examination of this situation, it becomes apparent that the screw threads possess a sharp geometry, causing the transferred load to concentrate on a very small contact area with the bone. Consequently, this leads to stress magnitudes surpassing the yield stress point of the bone and damaging its structure, similar to real-life conditions. Conversely, when considering other regions of the bone located away from the screw threads, stress values remain below the yield stress point, indicating no material failure (damage). Therefore, although the FoS values suggest signs of damage to the bony structures, it would not be appropriate to categorise it as resultant bone failure. These issues arise due to the occurrence of stress concentrations in areas with sharp geometries, and they do not have a negative impact on the overall integrity of the bone structure.

(Figure 5. Sample visual representation depicting excessive stress concentrations observed on the bone structures)

3.3. Fragment Contact and Bone Healing Issue

The simulation study also unveiled certain output parameters associated with the fracture contact surface, such as contact force based on contact pressure and interfragmentary movement between fracture fragments (relative fragment sliding and rotational angle). The sliding was determined by the distance between bone fragments acting on the fracture contact surface. As a rough calculation approach, assuming the contact surface resembles a geometric ellipse and the maximum rotation arc length equals the maximum sliding distance, the rotation of the fracture fragment can be approximated with reference to the ellipse axis length measured in the model. Additionally, the magnitudes of average surface contact pressure between fragments at the contact surface were derived from the simulation, and the corresponding contact force, based on contact pressure and fracture surface area, was computed. These outputs enabled assessment of the magnitudes of the compression effect of the fracture fragments on each other, as well as the fragment sliding and rotational angle on the fracture contact surface parameters that play a crucial role in bone fracture healing. Visual descriptions and double axis chart supported numerical results of the contact surface parameters are given in Figure 6.

(Figure 6. Visual descriptions and double axis chart supported numerical results of the contact surface parameters)

These simulation results indicated that the maximum values of the interfragmentary sliding distance, rotation, average contact pressure and contact force on the fracture surface were calculated from the simulation scenario FEA-006 as 0.367 mm, 0.560°, 0.449 MPa and 1217.059 N respectively. The results for pressure magnitude may exhibit some variation in the case of pre-loaded screw usage. Additionally, due to limitations in the FEA boundary condition setup procedure, the contact definition was established as a no separation contact type (without friction coefficient definition), meaning fragments can move against each other but separation of the fragments was not allowed. Nevertheless, even with this limitation, it would not be wrong to say that the simulation demonstrated logical outputs consistent with each scenario based on visual and numerical outputs under related assumptions.

Among these findings, sliding distance can serve as a crucial parameter in interpreting bone healing, as excessive interfragmentary movement can lead to delayed healing or non-union. Therefore, the primary objective in femoral neck fracture cases is to establish secure fixation [29]. The process of bone repair can be divided into three sequential phases: Inflammatory phase (1); Reparative phase (2); Remodelling phase (3) [30]. In the context of bone fracture healing, it is essential to consider direct (primary) and indirect (secondary) fracture healing. Indirect fracture healing does not necessitate anatomical reduction or rigidly stable conditions. In contrast, direct fracture healing requires the pursuit of union in the repair process, demanding absolute stability at the fracture site. Fractures healing via periosteal callus formation differ from intracapsular fractures, which are inherently more susceptible to non-union. As a result, achieving direct bone healing necessitates rigid stabilisation to inhibit callus formation in both cancellous and cortical bone [21]. Several studies emphasise that for direct fracture healing, the maximum sliding (interfragmentary movement) and the

maximum separation gap between fragments should fall within the range of 100-200 μm and 1.5° (0.02 rad), respectively [31–34]. If secondary fracture healing is the objective, movement of the fragments along the axes is beneficial for soft callus formation. However, it is crucial to keep the fracture gap and the amplitude of movement small (amplitude: 0.2 1 mm; fracture gap <2 mm) [35]. In the present study, the magnitudes of fragment sliding signify a displacement exceeding range of 100-200 μm in relation to the reference fragment movement for primary fracture healing. This data is derived from all scenarios conducted under pre-defined boundary conditions. The fundamental assumption regarding load-bearing was that the patient would be placing weight on their injured leg immediately following the surgical procedure for fracture fixation. It is imperative to interpret these findings judiciously, taking into account the assumptions made in the simulations, single stance with a loading magnitude of 2.69 BW on the femur head, and insights gained from clinical experiences, prior to making decisions regarding the fixation operation.

3.4. FEA Verification

During the internal verification procedures of the FEA setup, the relative difference between the applied force and the calculated reaction force values in the simulation were examined, as well as the mesh structure quality through a skewness metric check. The results revealed that the resultant applied force (1847 N) corresponded well to the resultant reaction force (1854 N) obtained from the simulation results, with a relatively small difference of 0.38%. The skewness metric assesses the deviation of elements from equilateral cells. A skewness value of 0 indicates perfect cell quality, while a value of 1 indicates fully degenerated cells (0: Equilateral; >0 to 0.25: excellent; 0.25 to 0.50: good; 0.50 to 0.75: fair; 0.75 to 0.9: poor; 0.9 to <1: bad; 1: degenerate) [36,37]. The FE model exhibited an average skewness metric value of 0.25±0.1, indicating excellent cell quality. In this perspective it can be said that although the findings of this study were not validated through cadaveric research, they still possess value and provide significant insights into the behaviour of different fixation scenarios utilising MAF as examined in this study.

Similarly, when evaluating the outputs of the FEA study, several factors were taken into consideration. This study has certain limitations, particularly concerning the methods employed in FEA. While FEA serves as a valuable supplementary tool for comprehending the mechanical behaviour of biological materials, it is susceptible to various errors during the analysis process [38]. Unfortunately, when considering multiple boundary conditions, the femur, which is a relatively intricate anatomical structure consisting of ligaments, muscles, and surrounding soft tissues, had its intricate anatomy simplified. Additionally, these simplifications may introduce numerical solution errors, which should be carefully interpreted in the context of real-life conditions. These factors also include the potential for unexpected and unpredictable dynamic conditions that may arise during actual operating conditions, limitations in simulating these conditions, the specific solution approach required for numerical methods, assumptions made to address these limitations, and the capabilities of the simulation solver platform to identify and address any anomalies in the results obtained. Despite the challenges associated with these factors, it was concluded that the FEM based analysis satisfactorily simulated the deformation conditions of the MAF-bone fixation. The simulation represented the expected response under predefined loading conditions. Consequently, the simulation results can be utilised to understand bone fracture fixation behaviour, improve the design, optimise the structure, and facilitate the production of the MAF used in this study.

4. CONCLUSIONS

This study aims to conduct a durability analysis of an innovative external fixator designed to address both stable and unstable proximal femoral fractures. The durability of this design was evaluated using engineering simulation techniques based on FEM based numerical analysis. The study successfully achieved its aim by providing a comprehensive description of parameters related to the deformation behaviour of the MAF. In the study, an average displacement value of approximately 7.4 mm was recorded for the MAF-bone fixation scenarios, potentially indicating improved stability compared to previous findings which reported displacement values ranging from 10 to 15 mm (a reduction of over 40% on average). The influence of leg support on the deformation behaviour of the MAF was found to be insignificant, and the structural stress results, along with calculated safety factors, indicated no material failure conditions for the MAF under predefined boundary conditions. In main conclusion, all results pertinent to the evaluation of durability in this study suggest that the proposed new MAF design operates safely and achieves the intended durability. However, in terms of direct fracture healing, the interfragmentary movement was observed to be relatively higher than the reference magnitude range of 100-200 μm for primary fracture healing. Considering the fundamental assumption related to load-bearing, it is presumed that the patient would bear weight (2.69 BW) on their injured leg immediately after the surgical procedure for fracture fixation. It is crucial to interpret this finding judiciously before deciding on the fixation operation, taking into account the assumptions made in the simulations. Additionally, it is recommended to conduct further studies to address the limitations associated with simulating the durability of the MAF. An experimental investigation for the physical validation of the design and a structural optimisation study focused on material saving should be undertaken to make final design decisions for future research. This study introduces a how-to-do simulation strategy tailored specifically for the MAF, which can be adapted for similar external fixators. These findings enhance our understanding of MAF durability and the stages involved in the design of medical implants.

Author Contributions: H.K.C.: Project administration, Investigation, Visualization, Formal analysis, Writing—original draft; M.I.: Data curation, methodology, Writing—original draft; H.O.: Conceptualization, Methodology, Resources; A.E.W.R.: Supervision, Writing—review and editing. All authors have read and agreed to the published version of the manuscript.

Funding: This article received partial support from The Scientific Research Projects Coordination Unit of Akdeniz University (Turkey).

Data Availability Statement: The data presented in this study are available in this article.

Conflicts of Interest: The authors declare no conflicts of interest. The funders had no role in the design of the study; in the collection, analyses, or interpretation of data; in the writing of the manuscript; or in the decision to publish the results.

REFERENCES

[1] Mittal, R., and Banerjee, S., 2012, "Proximal Femoral Fractures: Principles of Management and Review of Literature," J. Clin. Orthop. Trauma, **3**(1), pp. 15–23.

[2] Panteli, M., Rodham, P., and Giannoudis, P. V, 2015, "Biomechanical Rationale for Implant Choices in Femoral Neck Fracture Fixation in the Non-Elderly," Injury, **46**(3), pp. 445–452.

[3] Samsami, S., Saberi, S., Sadighi, S., and Rouhi, G., 2015, "Comparison of Three Fixation Methods for Femoral Neck Fracture in Young Adults: Experimental and Numerical Investigations," J. Med. Biol. Eng., **35**(5), pp. 566–579.

[4] Shen, M., Wang, C., Chen, H., Rui, Y., and Zhao, S., 2016, "An Update on the Pauwels Classification," J. Orthop. Surg. Res., **11**(1), p. 161.

[5] Nandi, S., 2021, "Revisiting Pauwels' Classification of Femoral Neck Fractures," World J. Orthop., **12**(11), pp. 811–815.

[6] Adanaş, C., and Özkan, S., 2019, "Comparison of External Fixation and Intramedullary Nailing in Geriatric Patients with Intertrochanteric Fractures of the Femur," J. Surg. Med., **3**(12), pp. 833–836.

[7] Catagni, M., Sdeek, M., Guerreschi, F., Lovisetti, L., and Tsibidakis, H., 2012, "Management of Proximal Femoral Fractures Using the Ilizarov Principles.," Acta Orthop. Belg., **78**(5), pp. 588–91.

[8] Ganz, R., Thomas, R. J., and Hammerle, C. P., 1979, "Trochanteric Fractures of the Femur. Treatment and Results.," Clin. Orthop. Relat. Res., (138), pp. 30–40.

[9] Kaufer, H., 1980, "Mechanics of the Treatment of Hip Injuries.," Clin. Orthop. Relat. Res., (146), pp. 53–61.

[10] Gotfried, Y., Frish, E., Mendes, D. G., and Roffman, M., 1985, "Intertrochanteric Fractures in High Risk Geriatric Patients Treated by External Fixation.," Orthopedics, **8**(6), pp. 769–774.

[11] Dhal, A., and Singh, S. S., 1996, "Biological Fixation of Subtrochanteric Fractures by External Fixation.," Injury, **27**(10), pp. 723–731.

[12] Christodoulou, N. A., and Sdrenias, C. V, 2000, "External Fixation of Select Intertrochanteric Fractures with Single Hip Screw.," Clin. Orthop. Relat. Res., (381), pp. 204–211.

[13] Moroni, A., Faldini, C., Pegreffi, F., Hoang-Kim, A., Vannini, F., and Giannini, S., 2005, "Dynamic Hip Screw Compared with External Fixation for Treatment of Osteoporotic Pertrochanteric Fractures. A Prospective, Randomized Study.," J. Bone Joint Surg. Am., **87**(4), pp. 753–759.

[14] Ozdemir, H., Urgüden, M., Dabak, T. K., and Söyüncü, Y., 2002, "Treatment of intertrochanteric femoral fractures with the use of a modular axial fixator device," Acta Orthop. Traumatol. Turc., **36**(5), pp. 375–83.

[15] Ozdemir, H., Dabak, T. K., Urguden, M., and Gur, S., 2003, "A Different Treatment Modality for Trochanteric Fractures of the Femur in Surgical High-Risk Patients: A Clinical Study of 44 Patients with 21-Month Follow-Up," Arch. Orthop. Trauma Surg., **123**(10), pp. 538–543.

[16] Ozdemir, H., Onder, Y., and Dabak, T. K., 2016, "Modular Axial Fixator Is a Reliable Method for Stable Proximal Femoral Fracture - A Finite Element Analysis and Mechanical Study," Akdeniz Med. J., **2**(2), pp. 63–73.

[17] Ye, Y., You, W., Zhu, W., Cui, J., Chen, K., and Wang, D., 2017, "The Applications of Finite Element Analysis

in Proximal Humeral Fractures," Comput. Math. Methods Med., **2017**, pp. 1–9.

[18] Lewis, G. S., Mischler, D., Wee, H., Reid, J. S., and Varga, P., 2021, "Finite Element Analysis of Fracture Fixation," Curr. Osteoporos. Rep., **19**(4), pp. 403–416.

[19] Saha, S., and Roychowdhury, A., 2009, "Application of the Finite Element Method in Orthopedic Implant Design.," J. Long. Term. Eff. Med. Implants, **19**(1), pp. 55–82.

[20] Heller, M. O., 2022, "Chapter 32 - Finite Element Analysis in Orthopedic Biomechanics," B. Innocenti, and F.B.T.-H.O.B. Galbusera, eds., Academic Press, pp. 637–658.

[21] Samsami, S., Augat, P., and Rouhi, G., 2019, "Stability of Femoral Neck Fracture Fixation: A Finite Element Analysis," Proc. Inst. Mech. Eng. Part H J. Eng. Med., **233**(9), pp. 892–900.

[22] Ugural, A. C., and Fenster, S. K., 2003, *Advanced Strength and Applied Elasticity*, Prentice Hall.

[23] Rembold, U., Nnaji, B. O., and Storr, A., 1993, *Computer Integrated Manufacturing and Engineering*, Addison-Wesley Pub. Co.

[24] Taddei, F., Pancanti, A., and Viceconti, M., 2004, "An Improved Method for the Automatic Mapping of Computed Tomography Numbers onto Finite Element Models," Med. Eng. Phys., **26**(1), pp. 61–69.

[25] Peng, L., Bai, J., Zeng, X., and Zhou, Y., 2006, "Comparison of Isotropic and Orthotropic Material Property Assignments on Femoral Finite Element Models under Two Loading Conditions," Med. Eng. Phys., **28**(3), pp. 227–233.

[26] Luo, S., Shen, X., Bai, X., Bai, J., Han, J., and Shang, Y., 2017, "Validation of Material Algorithms for Femur Remodelling Using Medical Image Data," Appl. Bionics Biomech., **2017**, pp. 1–10.

[27] MatWeb, 2023, "MatWeb: Online Materials Information Resource" [Online]. Available: https://www.matweb.com/.

[28] Eschweiler, J., Fieten, L., Dell'Anna, J., Kabir, K., Gravius, S., Tingart, M., and Radermacher, K., 2012, "Application and Evaluation of Biomechanical Models and Scores for the Planning of Total Hip Arthroplasty," Proc. Inst. Mech. Eng. Part H J. Eng. Med., **226**(12), pp. 955–967.

[29] Marsell, R., and Einhorn, T. A., 2011, "The Biology of Fracture Healing," Injury, **42**(6), pp. 551–555.

[30] Søballe, K., 1993, "Hydroxyapatite Ceramic Coating for Bone Implant Fixation," Acta Orthop. Scand., **64**(sup255), pp. 1–58.

[31] Fujie, H., Mabuchi, K., Yamamoto, M., and Sasada, S., 1988, "Negative Effect of Mechanical Stimulation of Fracture Healing.," Seikeigeka Biomech, **10**, pp. 21–25.

[32] Shapiro, F., 1988, "Cortical Bone Repair. The Relationship of the Lacunar-Canalicular System and Intercellular Gap Junctions to the Repair Process.," J. Bone Jt. Surg., **70**(7), pp. 1067–1081.

[33] Blecha, L. D., Zambelli, P. Y., Ramaniraka, N. A., Bourban, P.-E., Månson, J.-A., and Pioletti, D. P., 2005, "How Plate Positioning Impacts the Biomechanics of the Open Wedge Tibial Osteotomy; A Finite Element Analysis," Comput. Methods Biomech. Biomed. Engin., **8**(5), pp. 307–313.

[34] Yunus Emre, T., Kursat Celik, H., Arik, H. O., Rennie, A. E. W., and Kose, O., 2022, "Effect of Coronal Fracture Angle on the Stability of Screw Fixation in Medial Malleolar Fractures: A Finite Element Analysis," Proc. Inst.

Mech. Eng. Part H J. Eng. Med., **236**(6), pp. 825–840.

[35] Jagodzinski, M., and Krettek, C., 2007, "Effect of Mechanical Stability on Fracture Healing-an Update," Injury, **38**(1), pp. 3–10.

[36] ANSYS Product Doc., 2019, "ANSYS Meshing User's Guide: Skewness (Release 2019 R2)," ANSYS Inc., USA.

[37] Brys, G., Hubert, M., and Struyf, A., 2004, "A Robust Measure of Skewness," J. Comput. Graph. Stat., **13**(4), pp. 996–1017.

[38] Cheung, J. T. M., and Zhang, M., 2005, "A 3-Dimensional Finite Element Model of the Human Foot and Ankle for Insole Design," Arch. Phys. Med. Rehabil., **86**(2), pp. 353–358.

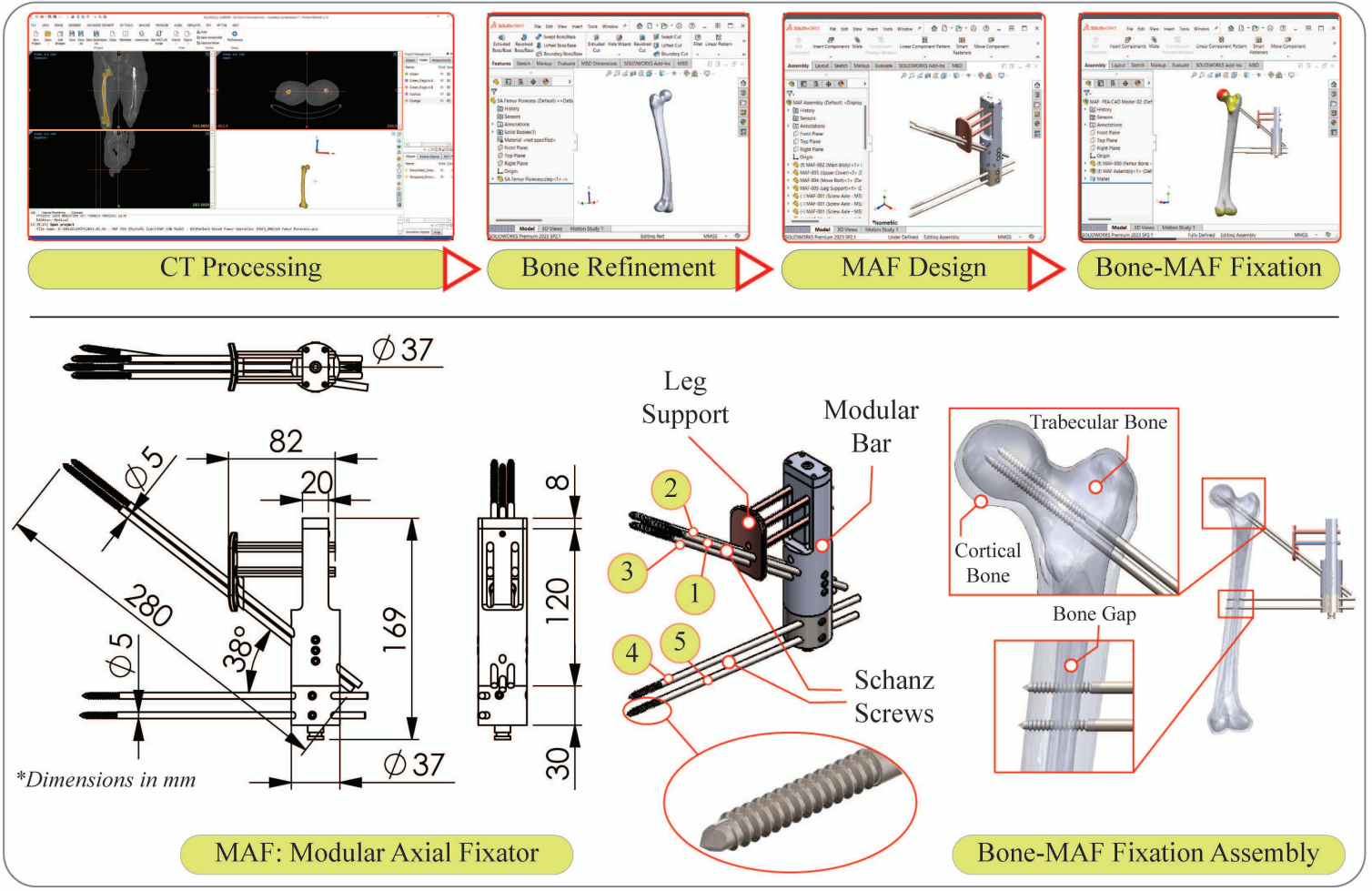

(Figure 1. Visual representation of the model details utilised in the FEA)

Boundary Conditions and Mesh Structure

A Fixed Support
B Force: 1.85e+003 N
C Standard Earth Gravity: 9.81e+003 mm/s²
θ: Corresponding angle (18.47°)

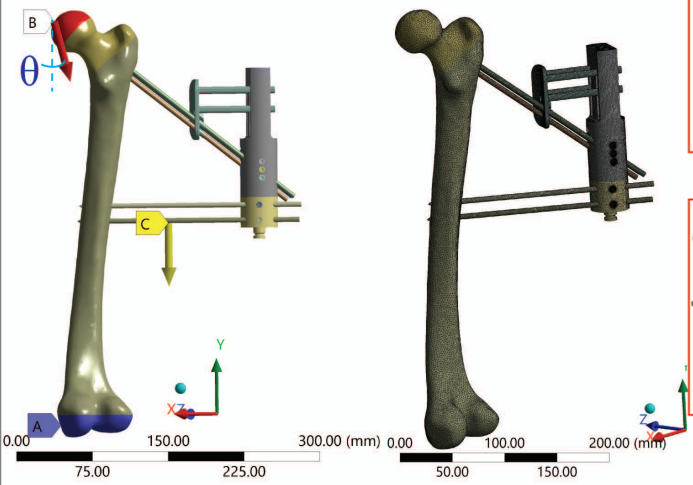

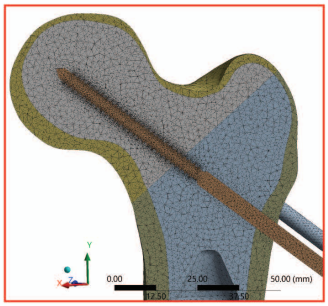

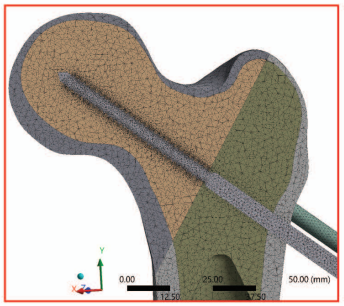

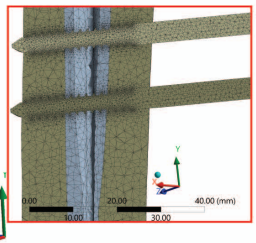

Details of the mesh structure (FE Model)		
Job Title	:	MAF - FEA
Meshing Approach	:	Part Based
Average Skewness Value / Quality Measure	:	0.25 ± 0.1 / EXCELLENT *
Element Types (ANSYS WB Code)	:	Tet10
Max. Element Size (body sizing) (mm)	:	8
Min. Element Size (mm)	:	1
Defeature Size (mm)	:	0.005
Element Growth Rate	:	1.5
Total Number of Elements	:	2401618 ± 86343 *
Total Number of Nodes	:	3639241 ± 131762 *

** Average value for eight FE models*

FEA Scenarios

Stable Fracture Fixation

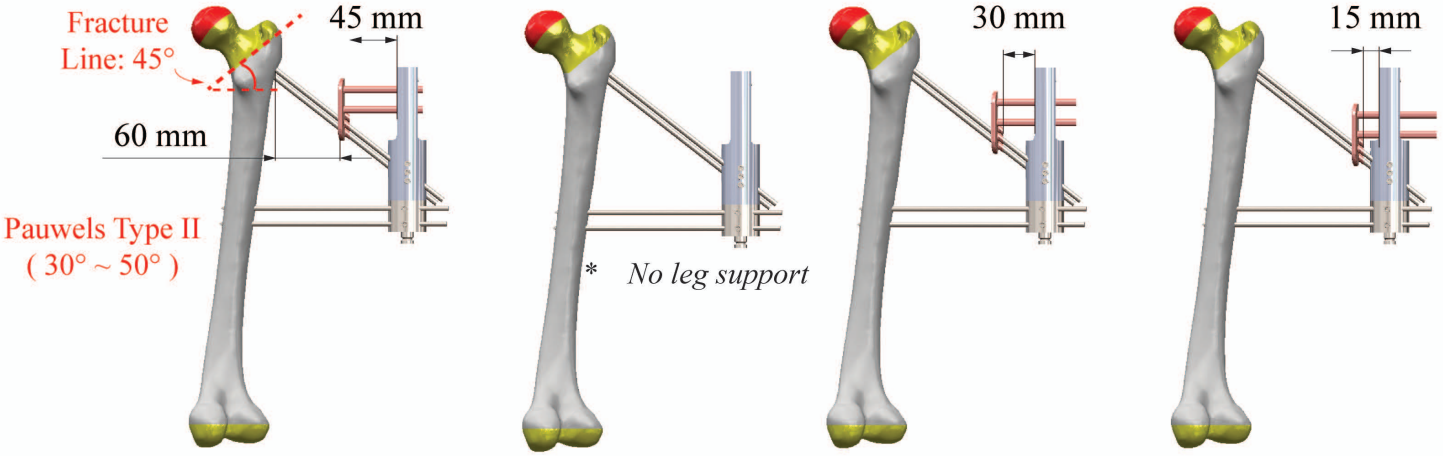

FEA-001 | FEA-001b | FEA-002 | FEA-003

Unstable Fracture Fixation

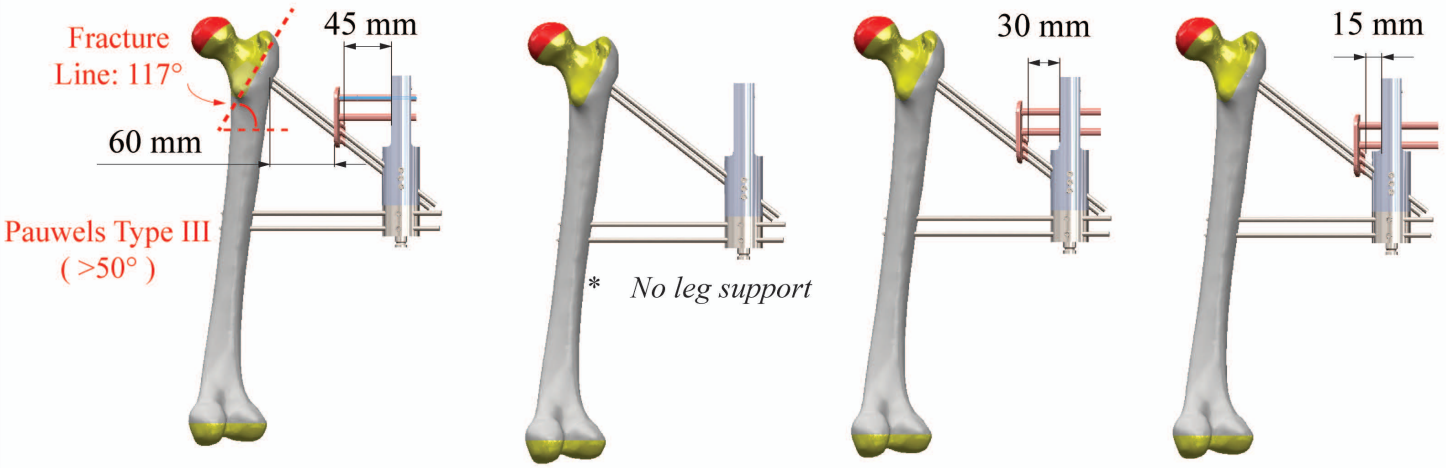

FEA-004 | FEA-004b | FEA-005 | FEA-006

(Figure 2. Depiction of the boundary conditions, details of the FE model (mesh Structure) and loading scenarios)

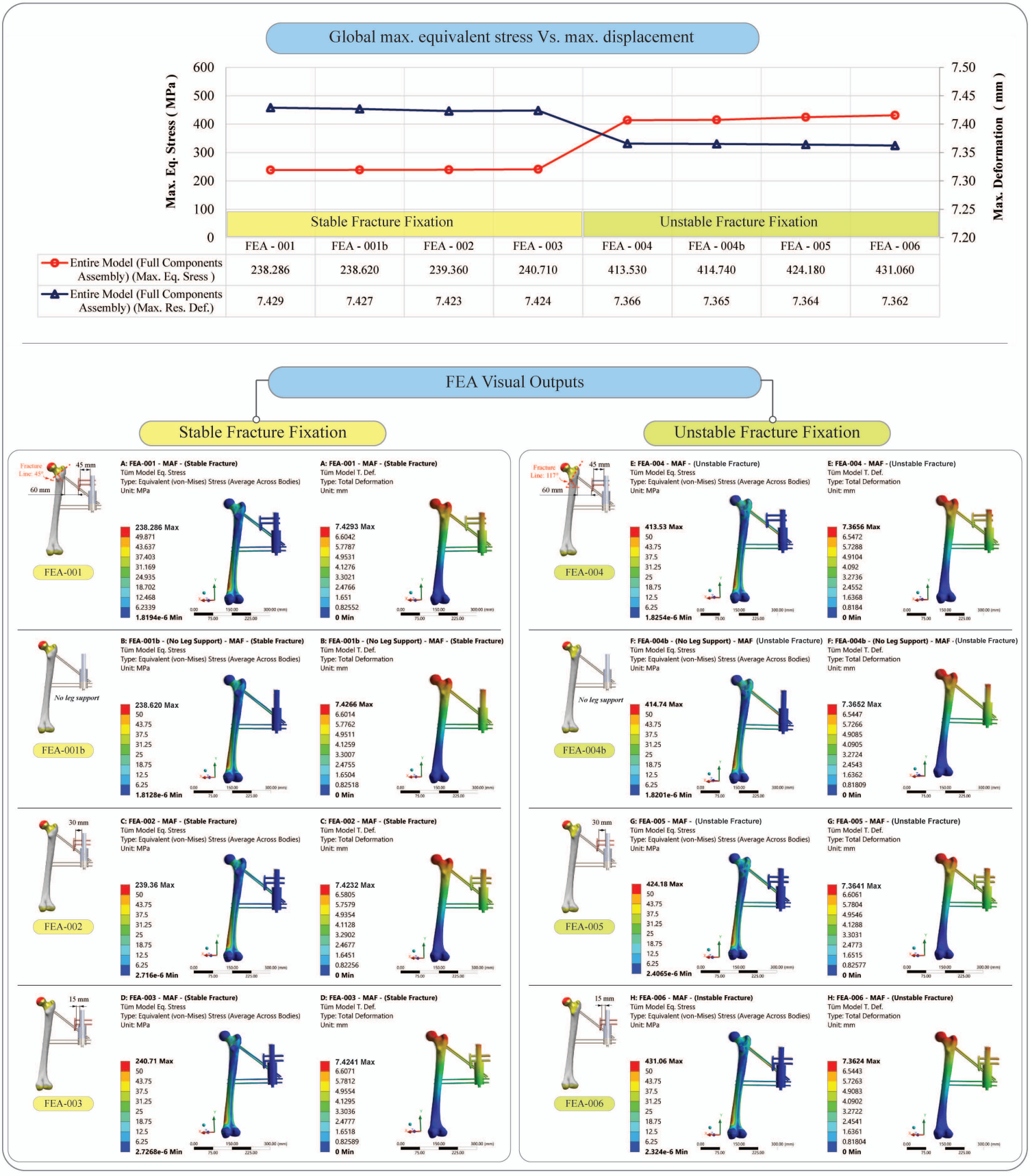

(Figure 3. Double axis chart representation and FEA visual outputs for global equivalent stress and displacement for stable and unstable fracture fixations)

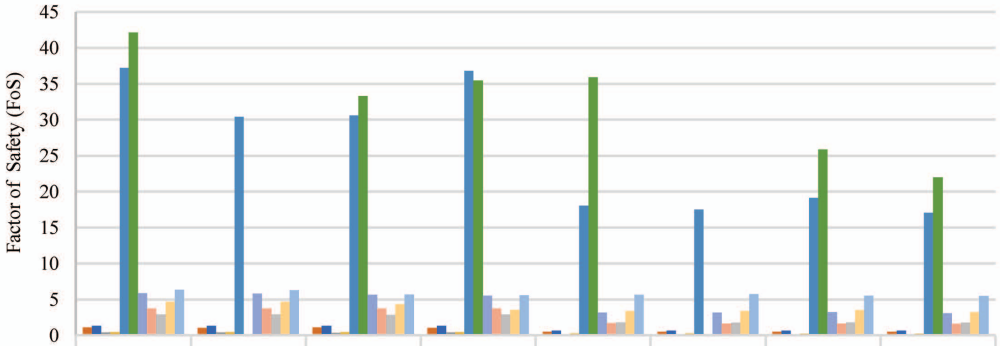

$$FoS = \frac{Material\ Yield\ Stress}{Calculated\ Stress}$$

Material's Yield Stress (MPa)		FEA - 001	FEA - 001b	FEA - 002	FEA - 003	FEA - 004	FEA - 004b	FEA - 005	FEA - 006
		Stable Fracture Fixation				Unstable Fracture Fixation			
165	Femur - Cortical Bone (Cortical Bone)	1.096	1.067	1.096	1.034	0.538	0.537	0.539	0.535
165	Femur - Cortical Bone -Fracture Segment (Cortical Bone)	1.349	1.337	1.346	1.335	0.667	0.666	0.679	0.663
30	Femur - Trabecular Bone (Trabecular Bone)	0.403	0.403	0.370	0.378	0.174	0.174	0.179	0.169
30	Femur - Trabecular Bone -Fracture Segment (Trabecular Bone)	0.460	0.460	0.458	0.450	0.313	0.310	0.262	0.259
560	Modular Bar (Aluminium 7075-T6)	37.202	30.413	30.638	36.765	18.066	17.522	19.169	17.073
560	Leg Support (Aluminium 7075-T6)	42.159	--	33.282	35.479	35.923	--	25.851	22.006
700	Schanz Screw No: 1 (Medical Grade S. Steel 316 LVM)	5.869	5.835	5.635	5.552	3.167	3.190	3.259	3.084
700	Schanz Screw No: 2 (Medical Grade S. Steel 316 LVM)	3.733	3.732	3.717	3.714	1.693	1.688	1.650	1.624
700	Schanz Screw No: 3 (Medical Grade S. Steel 316 LVM)	2.931	2.921	2.865	2.908	1.837	1.796	1.812	1.794
700	Schanz Screw No: 4 (Medical Grade S. Steel 316 LVM)	4.663	4.662	4.363	3.598	3.405	3.409	3.510	3.247
700	Schanz Screw No: 5 (Medical Grade S. Steel 316 LVM)	6.341	6.319	5.710	5.609	5.676	5.782	5.521	5.500

(Figure 4. Calculation of the factor of safety (FoS) by components)

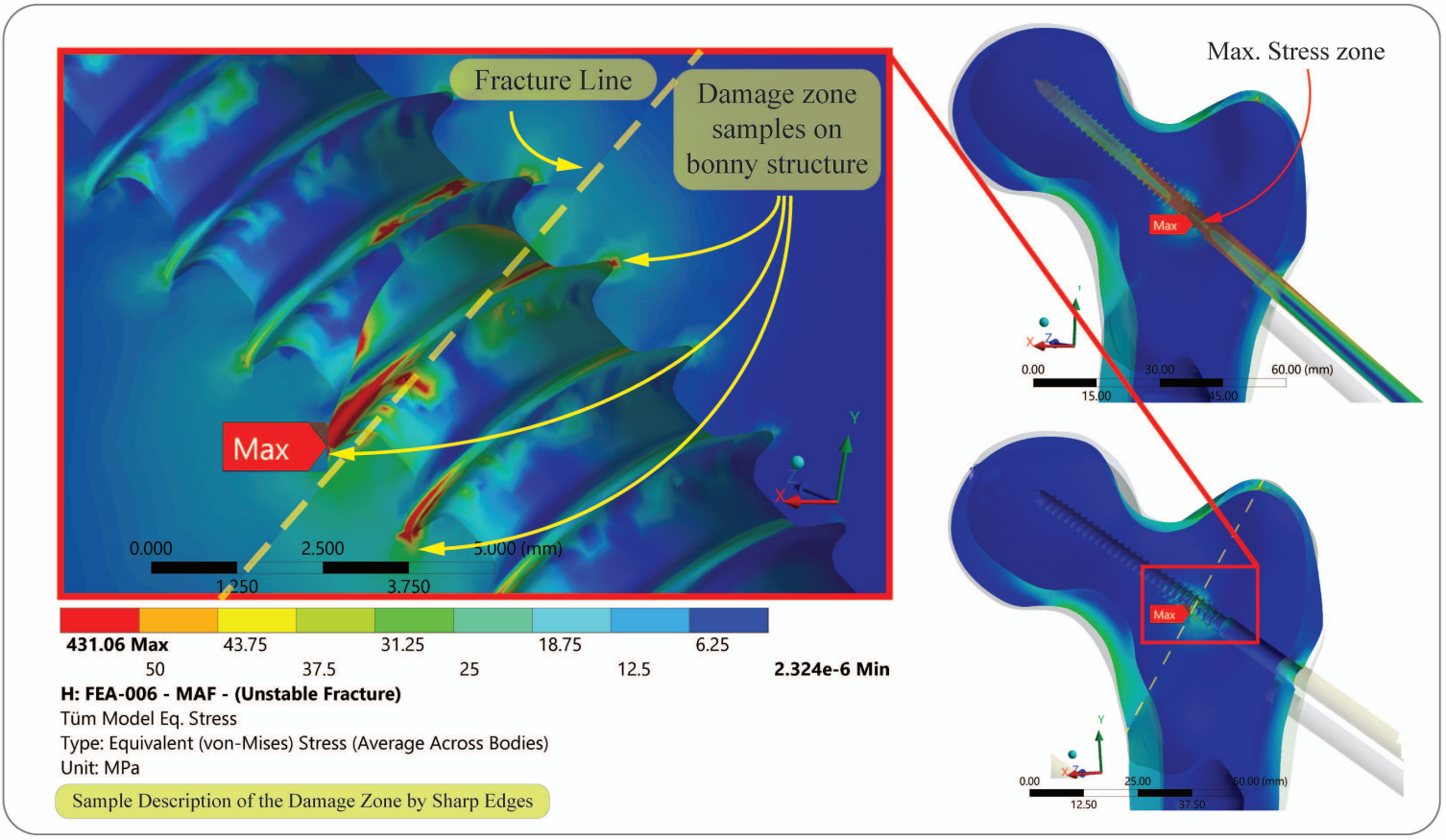

(Figure 5. Sample visual representation depicting excessive stress concentrations observed on the bone structures)

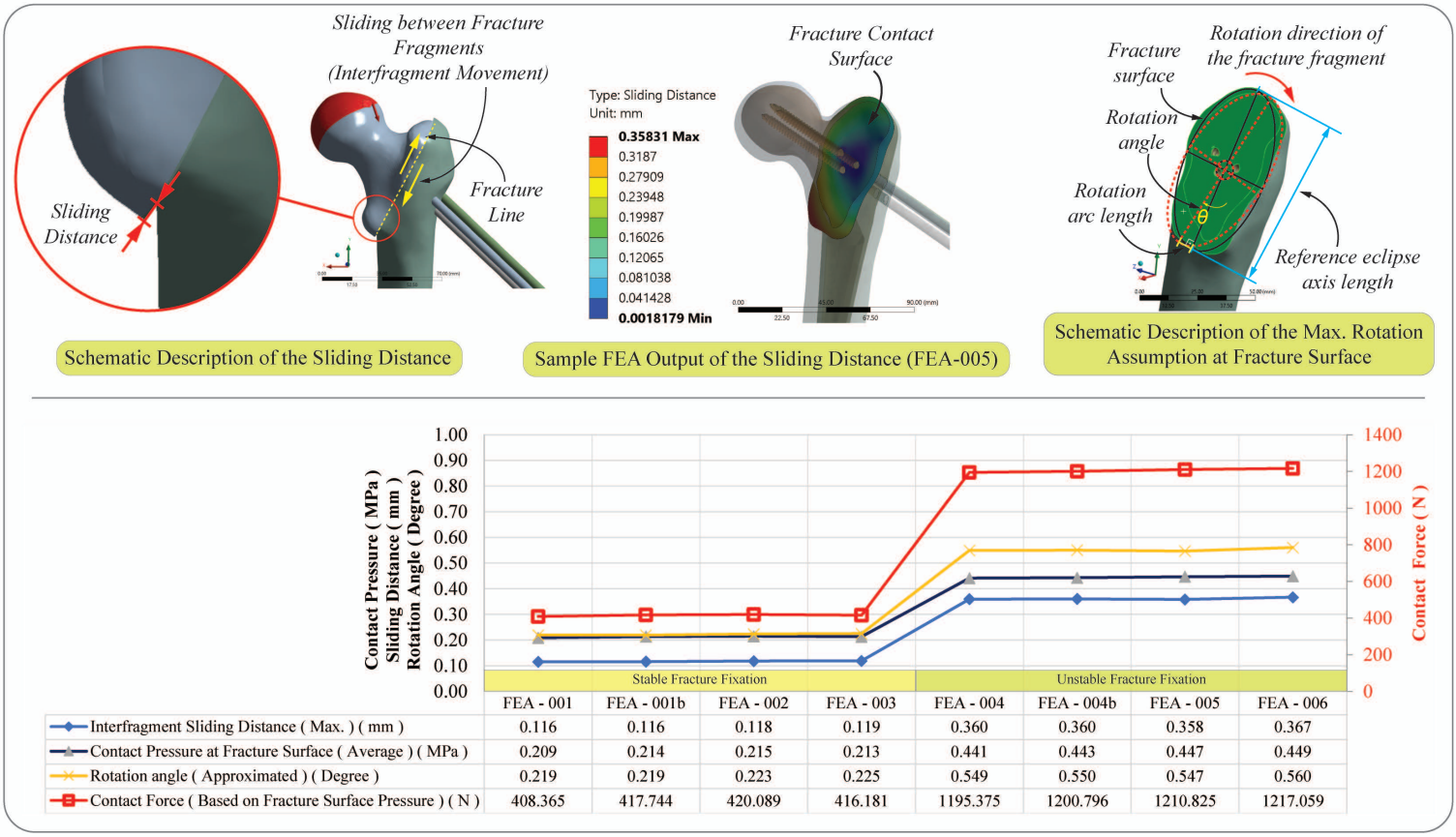

	FEA - 001	FEA - 001b	FEA - 002	FEA - 003	FEA - 004	FEA - 004b	FEA - 005	FEA - 006
Interfragment Sliding Distance (Max.) (mm)	0.116	0.116	0.118	0.119	0.360	0.360	0.358	0.367
Contact Pressure at Fracture Surface (Average) (MPa)	0.209	0.214	0.215	0.213	0.441	0.443	0.447	0.449
Rotation angle (Approximated) (Degree)	0.219	0.219	0.223	0.225	0.549	0.550	0.547	0.560
Contact Force (Based on Fracture Surface Pressure) (N)	408.365	417.744	420.089	416.181	1195.375	1200.796	1210.825	1217.059

(Figure 6. Visual descriptions and double axis chart supported numerical results of the contact surface parameters)

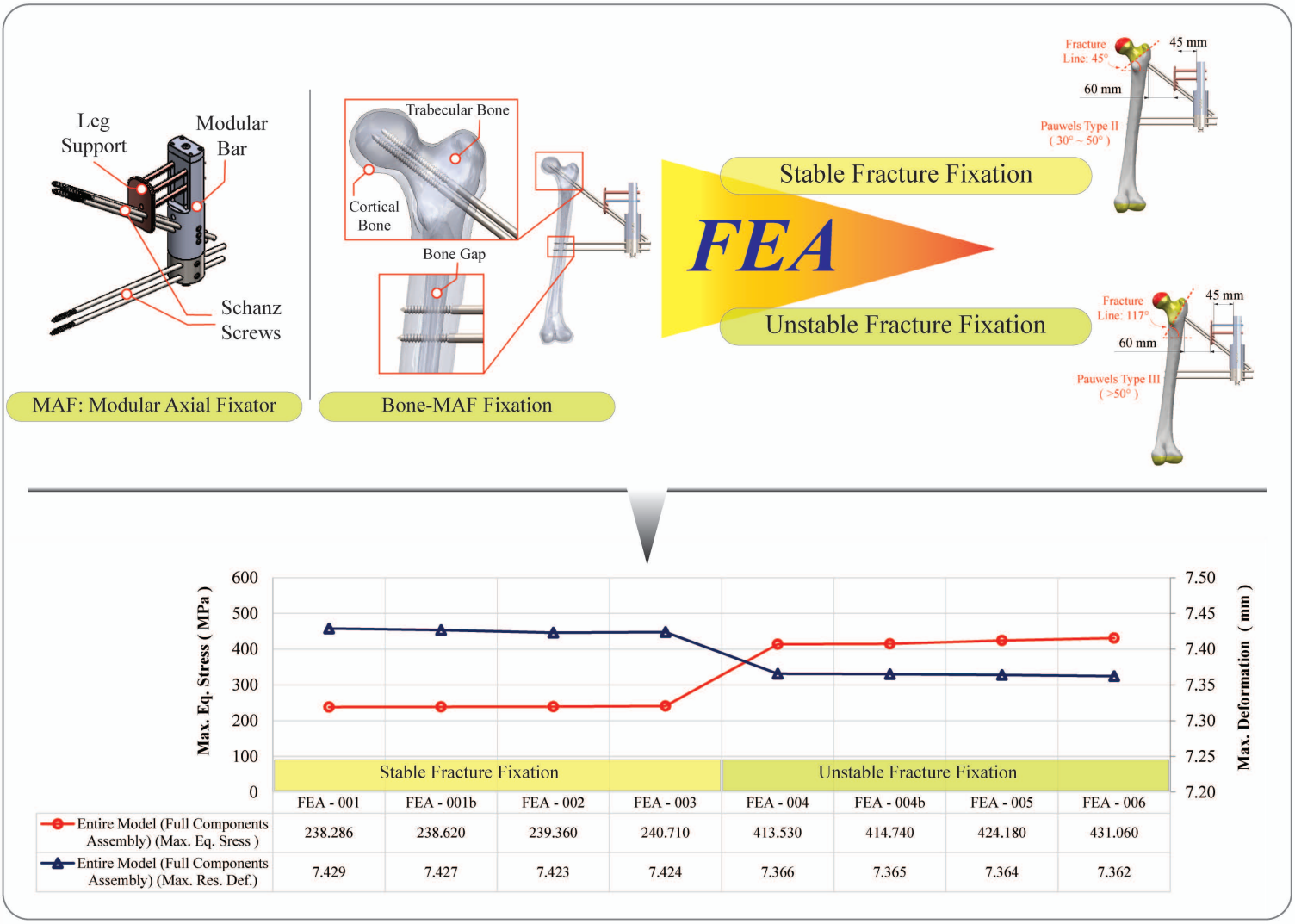

	FEA - 001	FEA - 001b	FEA - 002	FEA - 003	FEA - 004	FEA - 004b	FEA - 005	FEA - 006
Entire Model (Full Components Assembly) (Max. Eq. Sress)	238.286	238.620	239.360	240.710	413.530	414.740	424.180	431.060
Entire Model (Full Components Assembly) (Max. Res. Def.)	7.429	7.427	7.423	7.424	7.366	7.365	7.364	7.362

The ToC Graphic